Journal of Glaciology

Article

Cite this article: Shokory JAN, Lane SN (2023). Patterns and drivers of glacier debris-cover development in the Afghanistan Hindu Kush Himalaya. *Journal of Glaciology* **69**(277), 1260–1274. https://doi.org/10.1017/jog.2023.14

Received: 17 January 2022
Revised: 21 February 2023
Accepted: 25 February 2023
First published online: 5 April 2023

Keywords:
Afghanistan; glacier inventory; ice melt; principal component analysis; supraglacial debris

Author for correspondence:
Jamal A. N. Shokory,
E-mail: jamal.shokory@unil.ch

cambridge.org/jog

Patterns and drivers of glacier debris-cover development in the Afghanistan Hindu Kush Himalaya

Jamal A. N. Shokory and Stuart N. Lane

Institute of Earth Surface Dynamics (IDYST), University of Lausanne, CH-1015 Lausanne, Switzerland

Abstract

Debris-covered ice is widespread in mountain regions with debris an important control on surface ice melt and glacier retreat. Quantifying debris cover extent and its evolution through time over large regions remains a challenge. This study develops two Normalized Difference Supraglacial Debris Indices for mapping debris-covered ice based on thermal and near Infrared Landsat 8 bands. They were calibrated with field data. Validation suggests that they have a high level of accuracy. They are then applied to Landsat data for 2016 to produce the first detailed glacier inventory of the Afghanistan Hindu Kush Himalaya that includes debris cover. 3408 glaciers were identified which, for those $\geqslant 0.01\,km^2$ in area, gives an ice cover of $2{,}222 \pm 11\,km^2$ and a debris cover of $619 \pm 40\,km^2$. Principal components analysis was used to identify the most influential drivers of debris-covered ice extent. Lower proportions of debris cover were associated with glaciers with a higher elevation range, that were larger, longer and wider. These relations were statistically clearer when the dataset was broken down into climate and geological zones. A glaciers continue to shrink, the proportion of debris cover will become higher, making it more important to map debris cover reliably.

1. Introduction

Glacier inventories exist for most regions of the world (e.g. Bajracharya and Shrestha, 2011; Pfeffer and others, 2014; Nuimura and others, 2015; Mölg and others, 2018; Scherler and others, 2018; Herreid and Pellicciotti, 2020). These are generally based upon satellite imagery (Racoviteanu and others, 2009; Shukla and others, 2010). Clean ice can be mapped relatively easily, notably using thermal bands, though the threshold used to define ice cover needs calibration as they can vary both spatially and temporally (Veettil and others, 2014; Robson and others, 2015; Haireti and others, 2016). However, mapping debris covered ice remains a challenge (Bolch and Kamp, 2005; Raup and others, 2007; Racoviteanu and others, 2009; Mölg and others, 2018). Mountain glaciers can develop significant debris cover that can substantially modify glacier melt processes and response to climate warming (Nicholson and Benn, 2006; Jouvet and others, 2011; Scherler and others, 2011; Zhang and others, 2011; Pratap and others, 2015; Rowan and others, 2015; Vincent and others, 2016; Nicholson and others, 2018; Ferguson and Vieli, 2021).

Mapping debris covered ice from satellite imagery has made use of two primary approaches. The first is geomorphometric (e.g. Paul, 2003; Paul and others, 2004; Bolch and Kamp, 2006; Shukla and others, 2010; Bhardwaj and others, 2014; Veettil and others, 2014) where debris in ice marginal zones is classified as ice cored if local slope is below a certain threshold (the critical slope angle for debris movement). This may be problematic in some regions, such as where the transition from a glacier margin to an unglaciated region is gentle but still relatively debris free (Paul, 2003; Bolch and Kamp, 2006). In addition, no detectable change in surface slope may occur at the interface between clean-ice and debris-cover (Bhambri and others, 2011); post-depositional sedimentation by mass movement, a commonly found process in the polygenetic environment of the Himalaya (Benn and Owen, 2002; Bhambri and others, 2011), may cause confusion (Bhambri and others, 2011); and the available topographic data may not have the right resolution (Bolch and Kamp, 2006; Racoviteanu and others, 2009).

One alternative is to use differences in temperature between debris-covered ice and the temperature of the surrounding ice-free zones. Taschner and Ranzi (2002) analyzed the surface temperature and physical properties of both debris layers on glaciers and non ice containing zones (debris, rocks, grass) using ground measurements obtained for temperature and heat flux. They found significant temperature differences between debris-covered ice and other land surfaces with higher temperatures on average for surfaces without underlying ice. Amschwand and others (2021) recorded such differences to a debris thickness of 5 m. Subsequent studies have exploited this observation in satellite data. Scherler and others (2018), Herreid and Pellicciotti (2020) and Fleischer and others (2021) have used the proportion of near infrared (NIR) and shortwave infrared (SWIR) to map debris cover on glaciers. Stewart and others (2021) attempted to estimate debris thickness on glaciers using 60 m × 60 m Landsat Enhanced Thematic Mapper + data resampled to 30 m by 30 m. Herreid (2021) used ASTER data processed to give surface kinetic temperature at a 90 m resolution

and then used an unmixing approach to estimate the extent of debris-covered ice within a pixel, emphasizing the need for downscaling of the generally coarse thermal bands especially for mountain glaciers.

There are three issues that follow from these thermal band satellite based approaches. First, with very thick debris cover, the signal of ice temperature will diminish (Racoviteanu and others, 2009; Shukla and others, 2010) resulting in zones of debris-covered ice being classed as nonglacier. We assume that the importance of this problem is likely to increase with rapid glacier retreat, leading to potentially extensive areas of debris-covered ice that may be patchy and/or disconnected from the glacier itself. It emphasizes the need for further research to identify the limits of satellite-based estimation of debris-cover thickness. Second, following from the typical resolutions reported above, satellite-based studies have struggled to map small glaciers. Herreid and Pellicciotti (2020), for instance, excluded glaciers <1 km^2 even if for some mountainous regions a large proportion of glaciers fall in this class (Maharjan and others, 2018). One solution could be to downscale coarser thermal using higher resolution panchromatic bands as has been done in other applications (Choi, 2006; Aiazzi and others, 2007; Choi and others, 2010; Jung and Park, 2014; Rai and Mukherjee, 2021). Third, it is not yet clear whether or not a single index can map ice-covered debris regardless of the geological composition of such debris. If weathering processes lead to significant accumulation of fine-grained sediments on debris-covered glaciers then the debris cover will have small void spaces. This may result in greater capacity for water retention leading to wet surfaces (Juen and others, 2013; Blum and others, 2018) with different thermal properties to dry ones. As water and ice affect the thermal properties of a debris layer (Giese and others, 2020) more than one index may be needed to capture the spatial extent of debris-covered ice fully.

Given that debris cover remains a major cause of uncertainty in quantifying the retreat of glaciers in mountain regions (Scherler and others, 2011), there is a need for further development and testing of indices that can be used to map debris-covered ice in mountain regions, notably ones that can address the three issues identified above. Thus, the primary aim of this paper is to develop indices for mapping ice and debris-covered ice extent for mountainous regions that; (a) yield sufficient spatial resolution for mapping of valley-confined glaciers, including those < 1 km^2 in size; (b) are sensitive to geological controls on the caliber of accumulated sediment; (c) are suitable for long-term analyses so as to quantify change; and (d) use freely-available datasets.

The focus is on Afghanistan in the western part of Hindu Kush Himalaya where there remains only a poorly-developed understanding of the cryosphere despite its impact on both water resources and environmental hazards (Shokory and others, 2023). Most glaciological studies in Afghanistan are for the period 1965 to 1980 and are in Russian, Dutch and very occasionally English, and most are not available online (Shroder and Bishop, 2010). In 1980, Shroder initiated a glacier inventory for Afghanistan supported by the U.S. Geological Survey using Landsat-3 satellite imagery (40 m ground resolution), and field observations (Shroder and Bishop, 2010). This research identified about. 3000 separate glaciers in Afghanistan with an estimated area of about 2700 km^2 (Shroder, 1980; Shroder and Bishop, 2010; Shroder and Ahmadzai, 2016). A glacier inventory of Afghanistan was published by the Afghanistan Ministry of Energy and Water and International Centre for Integrated Mountain Development using satellite Landsat imagery (Maharjan and others, 2018). Glaciers were mapped using semi-automatic object-based image analysis methods and debris-covered ice was mapped using slope thresholds (0–24°). Maharjan and others (2018) identified 3782 glaciers, covering a total area of about. 2540 km^2 (excluding glaciers with an area of less than 0.01 km^2) concentrated at elevations between 3200 and 6900 m a.s.l. Thus, a subsidiary aim of the work is to produce a new glacier inventory for Afghanistan. As our method leads to one of the first inventories that can map very small (<1 km^2) glaciers, we seek to identify the regional-scale, systematic controls that explain spatial variation in debris-covered ice extent for Afghanistan using our inventory.

2. Study area

Afghanistan is a mountainous country located in the subtropics, extending from 29°21′N to 38°30′N latitude and from 60°31′E to 75°E longitude (Gopalakrishnan, 1982) (Fig. 1). It has an arid and semi-arid continental climate, characterized by temperature and precipitation regimes characteristic of deserts, steppe and highland environments (Humlum and others, 1959; Shroder, 2014). It has four main glacier regions (Fig. 1). We aim to produce a glacier inventory for all of Afghanistan. To support this work, we looked at two cases within Afghanistan in greater detail.

We undertook field data collection at the Mir Samir Glacier (Fig. 1) for index calibration and validation, which is the only glacier monitored by the Ministry of Energy and Water (MEW) of Afghanistan. This glacier is located at 70.171°N longitude and 35.596°E latitude (Fig. 1). Its highest altitude is 5060 m and it extends over a distance of 2.9 km to 4200 m altitude. The Mir Samir Glacier was mostly debris-covered in its snout zone, with some large boulders present. The proglacial margin also contains debris-covered ice. The geology around and under the glacier varies from slightly metamorphosed sedimentary rocks to hard gneisses and schists (Gilbert and others, 1969). This glacier was the primary focus of the first index we develop for mapping debris cover.

A second case, the Noshaq glacier range (Fig. 1) was also studied more intensively, albeit without a field visit. This glacier range was identified during the study as having debris-covered ice that was not being detected using our first index and so became the focus of the second index we developed. The Noshaq glacier range was studied in detail by Shroder (1978) (Fig. 1, Fig. S1, Supplementary Material). It contains one of the longest and largest glaciers in Afghanistan, starting from Noshaq peak, the highest peak in Afghanistan (7492 m) and extending for 14 km to an elevation of about 3580 m (Shroder, 1978) (location 36° 25′ N, 71° 47′ E).

3. Methodology

The approach makes use of freely available imagery from the Landsat 8 Operational Land Imager. The spatial resolution of its thermal bands is 90–120 m which creates particular uncertainty where clean ice and debris-covered ice are in juxtaposition (Bhambri and others, 2011; Kääb and others, 2014) or glaciers are small in size (<1 km^2). Thus, the two indices developed herein aim to improve the spatial resolution of thermal-based mapping and to resolve debris-covered ice where there is only a weak thermal signal.

3.1 Datasets

Data were obtained for ten L8 image tiles for the end of the 2016 ablation season (primarily in September) from http://earthexplorer.usgs.gov/ (Fig. S2, Supplementary Material), and on dates with no seasonal snow or cloud cover present in the scenes. The indices we developed used bands directly provided by

https://doi.org/10.1017/jog.2023.14 Published online by Cambridge University Press

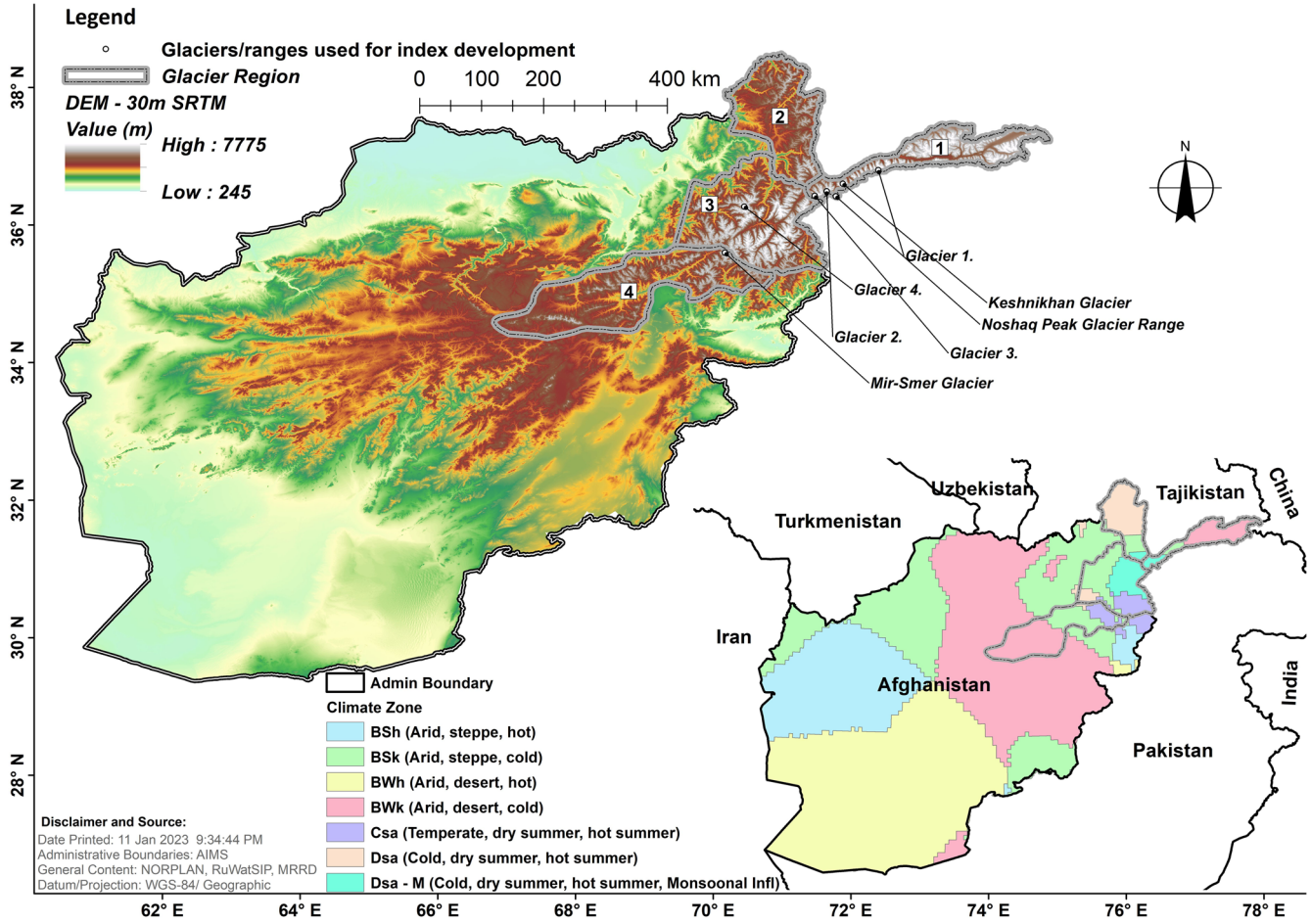

Fig. 1. Afghanistan showing the four glacier regions and their climatic zones (inset) based on the Köppen–Geiger climate classification (Peel and others, 2007) modified to include Dsa - M (Monsoonal influence) following Shroder (2014).

Landsat 8; blue-B2, near infrared (NIR)-B5, shortwave infrared (SWIR)-B6, panchromatic (PAN)-B8 and thermal (TIR)-B10. The B2, B5 and B6 bands have 30 m resolution, the B8 band 15 m resolution and the B10 band 100 m resolution that supplied already downscaled to 30 m. To correct for top of atmosphere reflectance, before all further analyses, we applied the radiometric rescaling coefficients provided in the associated metadata files delivered with the Landsat Level-1 NIR and SWIR products. We address the correction of PAN and TIR bands below.

Digital elevation models (DEMs) with resolutions of 5 m or 10 m (according to region) were provided by the Department of Statistics, Ministry of Agriculture Irrigation and Livestock of Afghanistan (MAIL, 2020). In areas where no Afghan DEMs were available we used 30 m resolution DEMs downloaded from the ALOS global digital surface model (ALOS, 2022). The Russian geological vector map of Afghanistan and high resolution (0.29 m) 2016-RGB images were obtained from Ministry of Mines and Petroleum of Afghanistan (MoMP, 2020).

3.2 Indices for mapping ice and debris cover

To map bare ice, we used the NIR to SWIR band ratio (Paul and others, 2002; 2004; Taschner and Ranzi, 2002; Paul, 2003; Bolch and Kamp, 2005; Shukla and others, 2010; Bhardwaj and others, 2014; Veettil and others, 2014). While methods for mapping debris-covered ice are available (see Supplementary Material), we develop a new index based upon a combination of L8 TIR and PAN bands. The principle behind this combination is that the TIR band is the one most likely to contain the thermal signal that allows identification of thicker debris layers. However, the L8 supplied TIR band is coarser (30 m). The PAN band is 15 m and, while theoretically less sensitive to thermal properties, it provides a means of downscaling the coarser TIR band to the resolution needed for mountain valley glaciers. This was done by assigning to each PAN value the nearest TIR value. The structural characteristics of debris-covered ice lead to a unique texture and panchromatic data have the potential to detect it (Bishop and others, 1995).

The PAN band has a reversed reflectance value (lower to higher) over debris to ice compared to TIR (higher to lower) (Fig. S3, Supplementary Material). On this basis we define a Normalized Difference Supraglacial Debris Index ($NDSDI_{c1}$):

$$\text{Normalized Difference Supraglacial Debris Indix } (NDSDI_{c1}) = \frac{\text{PAN} - \text{TIR}}{\text{PAN} + \text{TIR}} \quad (1)$$

During application we noted for a small number of glaciers in certain geological regions where the $NDSDI_{C1}$ suggested no debris-covered ice when there was likely to be ice present. Looking at the Russian geological map of Afghanistan (MoMP, 2020), we noted such regions were associated with detrital sedimentary rocks (mainly sandstone, siltstone, argillite, shale) (Shroder, 1980; Shroder and Bishop, 2010) which are highly erodible and result in smaller grain-size debris and likely wetter sediment. As the visible to near infrared single band ratio has been

https://doi.org/10.1017/jog.2023.14 Published online by Cambridge University Press

used previously to detect moist surfaces (Lobell and Asner, 2002; Amani and others, 2016), we use this to define a second index to capture ice covered by small-grained and moist debris:

$$\text{Normalized Difference Supraglacial Debris Indix } (NDSDI_{c2}) = \frac{\text{NIR}}{\text{Blue}} \quad (2)$$

3.3 Application of the indices

The indices were applied using the eCognition software (Trimble ©). Figure 2 shows the workflow for applying the indices and key steps are illustrated in Supplementary Material, Figure S4.

As an initial step, radiometric calibration was performed to convert digital numbers (DNs) for NIR and SWIR bands to reflectance values to map bare ice. Radiometric calibration and atmospheric correction was necessary for the NIR and SWIR bands (Fig. S4b, Supplementary Material). Radiometric calibration decreased the numerical range of NDSDI values during debris-covered ice mapping and also caused loss of resolution (Fig. S5, Supplementary Material). Thus, we used the original band DNs in (1) and (2).

Research has shown that misclassifications of pixels as debris-covered ice (e.g. Supplementary Material, Fig. S4d) can occur where there are steep debris-free slopes (Zollinger, 2003) and cold-water bodies. Following others (e.g. Bolch and others, 2007; Bhambri and others, 2011; Bhardwaj and others, 2014; Veettil and others, 2014), we first applied a local slope threshold of 37° on a pixel basis to remove bare rock surfaces but this did not eliminate the problem. Hence, we merged pixels into zones (clean ice, debris-covered ice, ice-free) and then calculated the mean slope of each debris-covered ice zone. The average value of slope was calculated by zone and those zones with slopes >24° were reclassified as ice-free.

Even with these thresholds, some areas of supposed debris-covered ice remained that were unlikely to be correct as they were too low in altitude compared with known glacier snout margins (Fig. S4e, Supplementary Material). For this we identified a minimum altitude threshold that differs based on each region (3500–4000 m a.s.l). Shadowed snow patches and bedrock misclassified as debris-covered were identified by using a minimum area (<0.01 km^2) of debris cover (following Tielidze and others, 2020). Lastly, some snow cover area was mapped as ice (e.g. Fig. S4i, Supplementary Material) and more recent imagery was used to identify and to remove such errors.

In summary, the following parameters need to be calculated and calibrated in our analyses: (1) a threshold for the NIR/SWIR ratio to identify clean ice; (2) threshold ranges for the two new indices of debris cover ice $NDSDI_{c1}$ and $NDSDI_{C2}$; (3) a slope threshold applied to merged debris-covered glacier zones to remove those erroneously identified as debris-covered ice; (4) a minimum altitude threshold; and (5) a minimum area threshold.

3.4 Calibration, validation and inventory comparison

Our approach to calibration and validation had six steps. First, we visually identified plausible parameter values and ranges by looking across a set of glaciers using the high resolution RGB image. For all parameters except the two NDSDI indices, the result was a set of plausible parameter values. For the two NDSDI indices it was plausible parameter ranges.

Second, we formally acquired field data for the Mir Samir glacier (Fig. 1) in September 2020, and randomly-selected a subset of this dataset to calibrate the ranges for the $NDSDI_{c1}$ index (Eqn (1)). Security issues meant we could only map one glacier, and even then we had to undertake field data collection with the support of armed guards. The Mir Samir Glacier is mostly debris-covered at its snout, with bigger boulders and potentially ice-cored debris in the proglacial margin. A total of 219 GPS points were collected under a stratified-random sampling approach using a Garmin GPSMAP 64s GPS (±3 meter positional uncertainty) from three ground types; clean ice zones, zones of debris-covered ice and nonice zones (Fig. S6, Supplementary Material). Thin and partially debris-covered ice was determined visually. Thicker debris-covered ice was identified by the presence of ice under large boulders. The full dataset was randomly divided in half for calibration and validation.

Third, as the field validation site for $NDSDI_{c1}$ did not include fine-grained sedimentary debris-cover, and required to validate $NDSDI_{c2}$ debris-cover classifications, we turned to the Noshaq range (Fig. 1). High resolution MoMP (2020) imagery was used to visually identify debris-covered ice by the presence of supraglacial ponds and crevasses (Bodin and others, 2010; Mölg and others, 2018). We then randomly selected points from ice-covered, debris-covered ice and nonice zones, which were also randomly separated into calibration and validation datasets.

Fourth, in order to assess the transferability of our approach, we manually mapped four other debris-covered glaciers in Afghanistan from the high resolution RGB imagery. We also tested our approach at the Santopath Glacier in the central Himalaya, India and the Khumbu Glacier in Nepal (Miles and others, 2018). Both sites have reliable published maps of debris-covered-ice. We applied our methodology (Fig. 2) to these glaciers.

Finally, we compared the glacier outlines of our study with datasets published by (1) Maharjan and others (2018) that used only a slope threshold >24° to identify debris-covered ice and the NDSI index for clean ice; (2) Scherler and others (2018) who used the Randolph Glacier Inventory (RGI) version 6.0 outline and then used 2013–2017 Landsat and 2015–2017 Sentinel optical satellite images to map where glaciers were debris-covered; and (3) Herreid and Pellicciotti (2020) who used the NIR/SWIR satellite band ratio to map debris cover and clean ice using Landsat data for 2013–2015. The outlines provided by Herreid and Pellicciotti (2020) came with on-line available datasets and so we also assessed their approach quantitatively for our 8 glaciers (two Afghan glacier used for calibration and validation; four additional glaciers in Afghanistan used for validation; and the Satopanth and Khumbu glaciers) where the datasets were available.

For both calibration and validation we used an error matrix approach (Congalton and Green, 2019) as used to evaluate land-cover classifications based on reference data (Foody, 2002; Congalton and Green, 2019). We calculated classical error statistics (total, user and producer accuracies) but also the Kappa statistic as the latter corrects accuracy assessments for chance agreement between classes (Lillesand and others, 2015). The commission errors define the user accuracy (i.e. the reliability of information derived from the classification; Story and Congalton, 1986) and so they can be used as proportional uncertainties to calculate uncertainty in mapped areas.

3.5 Inventory and exploration of controls on debris cover

We applied our methodology (Fig. 2) to all glaciers in Afghanistan to produce a new inventory. We then explored controls on debris cover percentage using Principal Components Analysis (PCA; Table 1). Catchments were identified using watershed delineation in ArcGIS at the outlet of each glacier. Catchment boundaries were then used to determine catchment area (1), and mean slope (2). Glacier length (3) was calculated following the Machguth and Huss (2014) method that determines and

https://doi.org/10.1017/jog.2023.14 Published online by Cambridge University Press

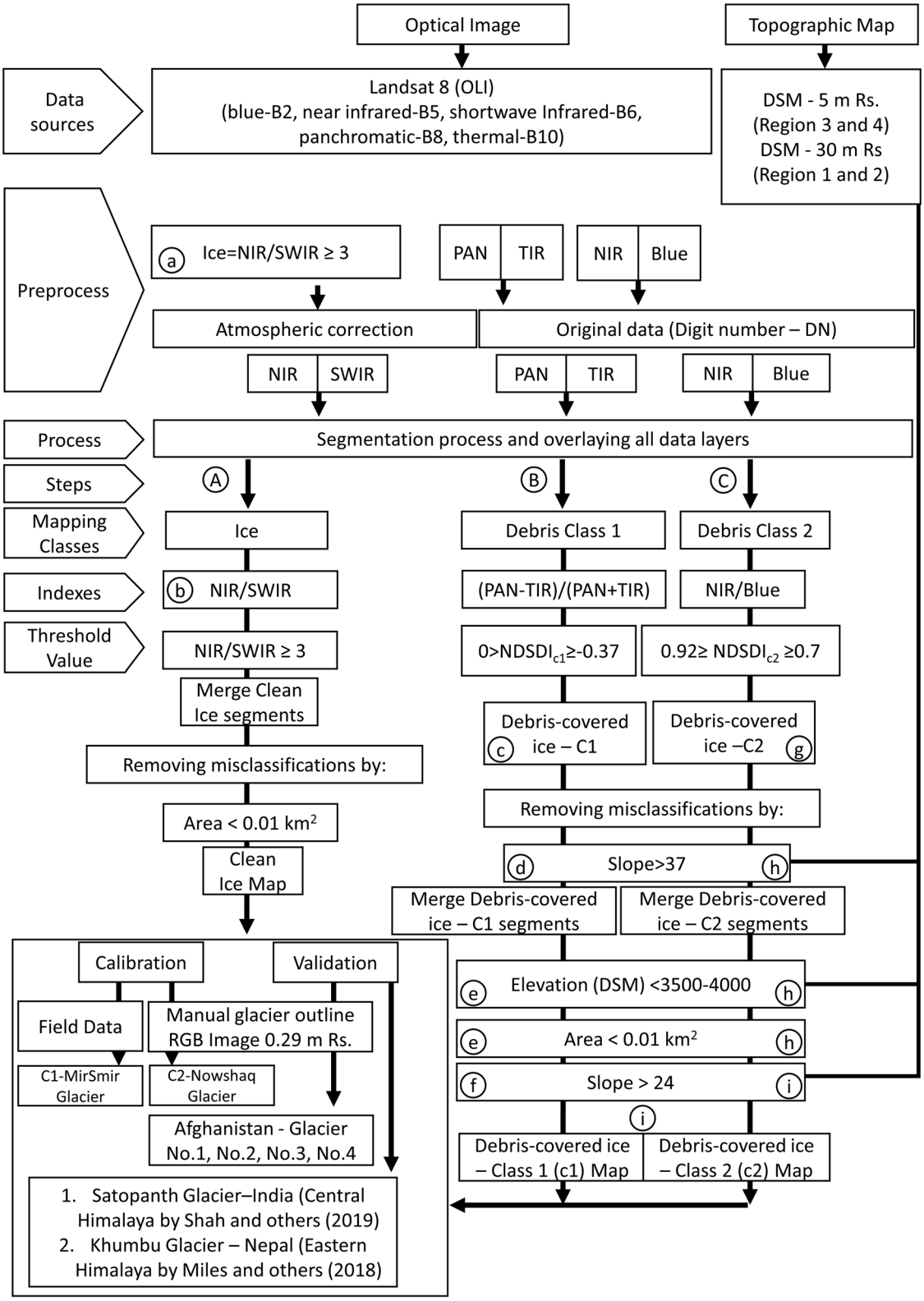

Fig. 2. Methodological steps used in the study. The letters shown link to Supplementary Material Figures S4a to S3i, DEMs used for each image tiles are showed in Supplementary Material Figure S2.

measures the centerline of the glaciers. However, for smaller glaciers (<0.07 km^2) we found that the method miscalculated glacier length as such glaciers often had their long axis tangential to the glacier surface slope rather than along it. For such glaciers, we used ArcGIS to calculate the longest distance between upper and lower points of the glacier. Herreid and Pellicciotti (2020) suggested determining glacier width as the linear distance orthogonal to glacier flow at the widest location of the main centerline. However, considering the complexity of glaciers in Afghanistan (Fig. 3) this method may not represent glacier width correctly. Thus, we calculated an effective glacier width (4) for individual glaciers by dividing glacier area to the glacier length. The debris influence area (5) was determined by intersecting each glacier outline with the glacier catchment outline (using the intersect toolbox in ArcGIS) and defining the influence area as that having altitudes higher than the lowest altitude of debris-covered ice.

https://doi.org/10.1017/jog.2023.14 Published online by Cambridge University Press

Table 1. Glacier parameters derived for the multivariate analysis

Parameter	Rationale
1 Catchment area	Catchment area is a scale effective variable with catchments with a smaller area likely to be more debris covered
2 Catchment mean slope	Steeper mean slope is likely to lead to valley sidewalls and headwalls where there is more debris supply by erosion
3 Glacier length	Longer glaciers are likely to have proportionally less headwall debris delivery
4 Glacier mean width	Wider glaciers are likely to have proportionately less sidewall debris delivery
5 Debris influence area	The area of a catchment containing a glacier that is not ice covered or debris-covered ice, representing a measure of potential debris supply
6 Glacier mean elevation	Higher glaciers have higher accumulation and lower ablation so reducing debris cover at the surface
7 Glacier elevation range	Glaciers with a bigger elevation range are likely to have a more extensive accumulation zone, so reducing debris cover at the surface
8 Glacier mean slope	Steeper glaciers are likely to encourage less debris accumulation
9 Geological hardness grade	A measure of the resistance to erosion and hence inversely related to potential debris supply
10 Climatic zone	Geographical classification to capture different potential climatic influences on temperature and precipitation and hence accumulation and ablation.

The DEM was used with the glacier boundaries to calculate glacier mean elevation (6), glacier elevation range (7) and glacier mean slope (8) using the zonal statistic tool in ArcGIS. The geological information for each glacier (9) was extracted from the geological map of Afghanistan provided by the Ministry of Mines and Petroleum of Afghanistan (MoMP, 2020). The geological information consists of 27 geological type grouped into 6 geological categories. In addition, the Köppen-Geiger climate classification (Peel and others, 2007) was used to represent the climate characteristics of the glaciers.

Due to potential inter-correlation between these variables, PCA was used to reduce this dataset to a set of linearly independent principal components (PCs) that were then used to explain the statistical controls on debris cover (Gupta and others, 2013; Ghosh and others, 2014). First, we standardized the data by dividing each variable by its standard deviation. Second, the PCA was applied and the variance and factor loadings were calculated (Jensen, 1996; Ghosh and others, 2014). Orthogonal rotation (orthomax) that maximizes a criterion based on the variance of the loadings was used to simplify the interpretation of the resulting factors, and to ensure that the components remained pairwise uncorrelated for subsequent linear modeling. We used a 5% contribution to the original data variance as the cut off for retaining a component. We then interpreted each component with respect to its loadings.

Finally, we established relationships between percentage of debris cover and the new PCs. For this purpose, we used an optimizing stepwise regression where components were added to the model in order of decreasing importance provided that their individual contribution to the total explanation of the model was significant at $p < 0.05$. We undertook this modeling for both the entire dataset, but also the dataset divided in two ways: by climatic zones and by geological classes.

4. Results

4.1 Index calibration, validation and comparison

For the clean ice NIR/SWIR threshold, visual comparison of results with the imagery suggested that a value of NIR/SWIR ⩾3 appeared to map clean ice effectively. The mean zonal slope for the removal of zones (not pixels) misclassified as debris-covered ice was 24°. We found that an elevation threshold altitude of <3500 m for regions 2, 3 and 4 and altitude <4000 m for region 1 (Fig. 1) was appropriate for the minimum altitude condition (Supplementary Material, Fig. S4 e,h). Finally, we removed zones classified as glacier or debris-covered glacier <0.01 km^2 if detached from ice and/or debris-covered ice (Supplementary Material, Fig. S4 e,i). The visual analysis suggested the following two parameter ranges for debris covered ice $0 > \mathrm{NDSDI}_{C1} \geqslant -0.32$; and $0.88 \geqslant \mathrm{NDSDI}_{C2} \geqslant 0.70$.

Based on the ground observations from glacier, pixels with $\mathrm{NDSDI}_{C1} \geqslant -0.37$ were classified as debris-covered and was optimal, therefore adopted for this study. The calibration accuracy assessment (Table 2) gave very encouraging results; the overall accuracy was 0.98 and the Kappa coefficient was 0.91. For the second index, a range of $0.92 \geqslant \mathrm{NDSDI}_{C2} \geqslant 0.70$ was chosen to maximize the accuracy of the approach. The overall accuracy for the Noshaq glacier range was 0.92 and the Kappa coefficient for both clean ice and debris-covered ice was 0.91 (Table 2).

Table 3 shows the validation results for the Mir Samir and the Noshaq glaciers and also for the four other glaciers considered in Afghanistan and the two outside of Afghanistan (Fig. S7 Supplementary Material). The results are encouraging as there is only a very slight degradation in the overall accuracy and the Kappa coefficient in transferring the calibrated index both within and between glaciers.

For the Afghan glaciers 1–4 (Fig. 3) the extent of debris-covered ice in the glacier marginal zone is revealed by supraglacial ponds and crevasses and these zones tend to be missed in part by other inventories as compared with our method (Fig. 3, Glacier 2). Compared with the Herreid and Pellicciotti (2020) approach, we obtained higher Kappa coefficient accuracy with our method for Glacier 1 (0.95 and 0.96 for clean ice and debris-covered ice respectively as compared to 0.77 and 0.78 respectively) mainly due to better estimation of ice presence in the margin of the glacier (Fig. 3, Glacier 1). Similarly, for Glacier 3, debris cover ice was missed around the terminus and margins by the Herreid and Pellicciotti (2020) index resulting also in lower accuracies and Kappa coefficients (Table 3).

Our method also shows higher accuracies level for those glaciers outside of Afghanistan in the Himalaya (Table 3). We obtained 0.94 Kappa accuracy for clean ice and debris cover ice for both glaciers using our method. The Herreid and Pellicciotti (2020) index gives lower values for both the Satopanth glacier and the Khumbu glacier.

4.2 Glacier inventory

We identified (Table 4) 3408 glaciers which, considering those ⩾0.01 km^2, sums to 2,222 ± 11 km^2 of ice cover, 619 ± 40 km^2 of debris-covered ice and glacier surface areas up to 21.2 km^2. Differences in the number of glaciers by region varied reflecting different climatic, elevation and geological zones. Region 1 has the highest number of glaciers, with a larger mean and variability of glacier area (1.21 ± 2.25 km^2). The percentage of debris-covered ice is highest in Region 4 (42%) where there are also fewer and smaller glaciers. Regions 1, 2, 3 and 4 have 69%, 4%, 25% and 2% of the total debris cover. The glaciers differ markedly in altitudinal range (Table 4).

https://doi.org/10.1017/jog.2023.14 Published online by Cambridge University Press

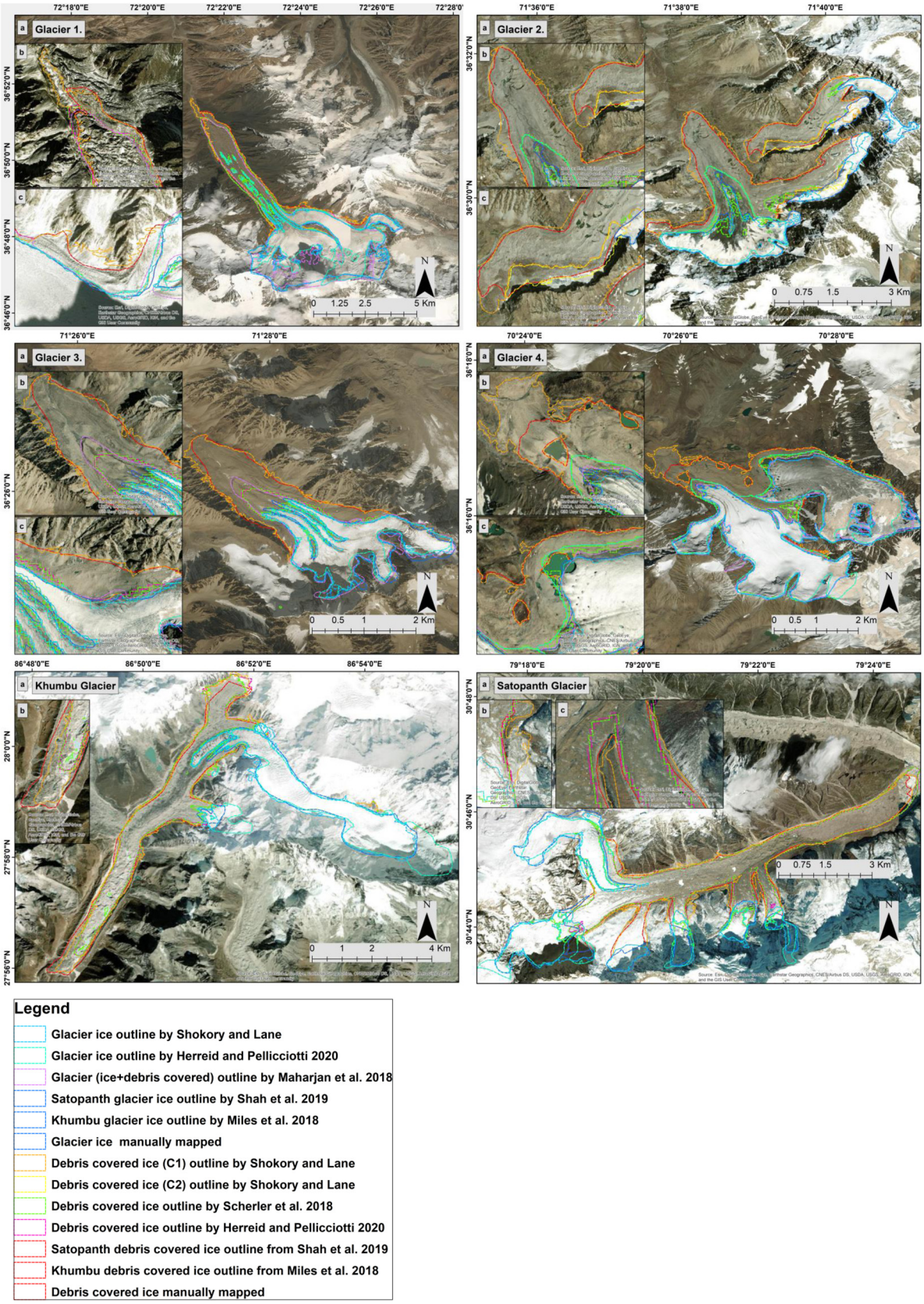

Fig. 3. Comparison of the index results for Afghanistan glaciers 1 to 4 and the Satopanth and Khumbu glaciers with those using other indices. Blue and red outlines used as reference outlines.

There is a clear regional association in both size and debris cover (Fig. 4) and these associations were significant (Kruskal–Wallis H, $p < 0.05$).

Hypsometric distributions (Fig. 5) suggest that glaciers are distributed between 3500 and 7380 m a.s.l, but that debris-covered ice is limited to altitudes below 5500 m. There is between region-variability. Glaciers in Region 1 and 3 concentrate on 5000 m a.s.l altitude and Region 2 and 4 on 4500 m a.s.l. Comparing glacier elevation ranges, Region 1 and 3 are at higher elevations than Region 2 and 4 (Table 4). This shows a

https://doi.org/10.1017/jog.2023.14 Published online by Cambridge University Press

Table 2. Calibration results for the Mir Samir and Noshaq glaciers

Accuracies	Clean ice	Debris-covered ice	Not ice
Mir Samir glacier: overall accuracy 0.98			
Commission error (Com)	0.02	0.09	0.00
Producer's accuracy (PrAc)	0.98	0.91	1.00
Omission error (Om)	0.01	0.17	0.00
User's accuracy (UsAc)	0.99	0.83	1.00
Kappa coefficient	0.92	0.98	0.98
Noshaq glacier: overall accuracy 0.92			
Commission error (Com)	0.12	0.14	0.06
Producer's accuracy (PrAc)	0.88	0.86	0.94
Omission error (Om)	0.08	0.18	0.07
User's accuracy (UsAc)	0.92	0.82	0.94
Kappa coefficient	0.91	0.91	0.86

Table 3. Validation results and comparison with the Herreid and Pellicciotti (2020) index

		Producer's accuracy (PrAc)		User's accuracy (UsAc)		Kappa coefficient	
Validation datasets	Overall Accuracy (OcAc)	Ice	Debris cover	Ice	Debris cover	Ice	Debris cover
Indices used in this paper							
Mir Smir Glacier, Image 8	0.98	0.99	0.88	0.99	0.88	0.92	0.98
Noshaq Glacier, Image 5	0.93	0.88	0.85	0.92	0.82	0.92	0.93
Glacier 1, Image 3	0.96	0.98	0.93	0.96	0.89	0.95	0.96
Glacier 2, Image 6	0.89	0.99	0.85	0.75	0.97	0.89	0.87
Glacier 3, Image 6	0.94	0.95	0.86	0.85	0.96	0.94	0.94
Glacier 4, Image 6	0.95	0.98	0.79	0.95	0.96	0.94	0.95
Satopanth Glacier, India	0.94	0.83	0.91	0.91	0.90	0.94	0.94
Khumbu Glacier, Nepal	0.94	0.91	0.87	0.90	0.92	0.94	0.93
Herreid and Pellicciotti (2020) *inventory*							
Mir Smir Glacier	Not included in Herreid and Pellicciotti (2020) inventory						
Noshaq Glacier	0.81	0.80	0.90	0.41	0.59	0.81	0.81
Glacier 1	0.79	0.89	0.89	0.58	0.68	0.77	0.78
Glacier 2	Not included in Herreid and Pellicciotti (2020) inventory						
Glacier 3	0.79	0.91	0.73	0.78	0.18	0.78	0.79
Glacier 4	Not included in Herreid and Pellicciotti (2020) inventory						
Satopanth Glacier	0.90	0.84	0.89	0.71	0.79	0.90	0.89
Khumbu Glacier	0.89	0.75	0.87	0.89	0.83	0.88	0.88

clear signal of altitudinal effects on glacier distribution in Afghanistan.

Regions 1 and 3 tend to have larger glaciers than 2 and 4 (Fig. 6). The percentage debris-covered ice shows significant correlation with glacier size; smaller glaciers have more debris-covered ice than larger glaciers, notably for Regions 1, 2 and 3. The relation is nonlinear to varying degrees and heteroscedastic (Fig. 5), small glaciers in Region 2 and 3 in particular having disproportionately higher percentage debris cover but also a greater range of debris cover.

The median aspect ratio of glaciers at four sub glacier regions in Afghanistan was oriented towards the northeast and northwest (Fig. S8, Supplementary Material).

4.3 Drivers of debris cover based on PCA-based analysis

The initial attempt to identify controls on debris cover fractions considers the complete glacier database. The PCA identified five PCs that represented 72% of the original dataset (Table 5). Only components with significance loadings were included in the stepwise regression. The latter used percentage debris-covered ice as the dependent variable (Table 5) which had a resultant R^2 of 43.7%.

There are six variables that contribute to the PCs (Table 5) and each PC is then labeled based on these contributions (Table 6). The first most important component identified in the regression was PC2 which is associated with variables that describe glacier length and elevation range. It explained 19.1% of the original data and was negatively associated with percentage debris cover. Thus, larger glaciers with greater elevation ranges tend to have lower percentage debris-covered ice. The second most important component ranked was PC4, which represented glacier width and which explained 12% of total variability in original data (Table 6). This suggests that wider glaciers have lower percentage debris-covered ice. The third most important component ranked was PC3, which represented glacier/catchment slope parameters and which explained 16% of the total variability in the original data (Table 6). The sign of association suggests that steeper glaciers are more prone to higher percentage debris-covered ice. PC1 that corresponds to catchment size explained 22% of total variability in the original data but was not included in the stepwise regression.

Given the possibility of strong spatial dependence in these analyses associated with broad-scale regional controls (e.g. climate, geology), it is possible that analysis of the entire dataset masks underlying drivers of debris cover. Thus, we undertook the same analysis but by climate zone and geological region. The Tables S2 and S3 in Supplementary Material contain the full results and we only present summary tables here.

A consistency and coherence in terms of the sign of the association of individual PCs and debris cover was found in general for all datasets whether classified by climate or geology; although there were some differences, such as in the details of the variables that contributed to each component.

For all climate zones, the PC that is associated with glacier length and elevation range is ranked as the most or second most important component (Table 7). PCs associated with glacier width are ranked as the second or third most important component. They are negatively associated with percentage debris cover through all climate zones and suggest that longer and wider glaciers have less debris-covered ice. Glacier altitude is ranked as the most important in climate zones 2 and 4 and the fourth most important component in climate zone 1, but is not significant in zones 3 and 5. Glacier altitude is negatively associated with percentage debris cover, suggesting higher altitude glaciers have proportionately less debris-covered ice. The glacier/catchment slope component is positively associated with debris cover in all climate zones, ranked as the second most important component in zone 3, the third most important component in zones 1, 4 and 5 and the fourth in zone 2. The sign suggests that steeper ice and catchment slopes lead to greater percentage debris cover. Catchment size in zones 2, 3 and 4 was not included in the stepwise regression. However in zone 1 it was ranked the fifth most important component with a positive association; and in zone 5 it was ranked as the fourth most important component with a negative association. The positive sign of association suggests that bigger catchment areas have higher percentage debris cover. However, the negative sign of association may be due to the fact that catchment size is also related to glacier length, width and elevation range parameters. This indicates that longer and wider glaciers are associated with larger catchments, and therefore negatively associated with percentage debris-covered ice.

Table 8 shows the results when glaciers are classified into the six geological categories. This classification leads to higher levels of explanation (R^2) for some classes as compared with modeling using the full dataset or divided into climatic zones. It suggests that the assumed linear ranking of resistance to erosion used for the full dataset does not represent geological effects well and that once divided into geological zones, geological controls on

https://doi.org/10.1017/jog.2023.14 Published online by Cambridge University Press

Table 4. Summarize the glacier inventory of Afghanistan for 2016

Glacier regions	Glacier elevation range (m)	Glacier cover for this elevation range (%)	No. of glaciers	Ice cover (km^2)	Debris-covered ice extent (km^2)	Mean glacier size (km^2)	Percentage debris cover (%)
R1- Northeast	3800-7380	18	1499	1397 ± 7	426 ± 25.6	1.21 ± 2.25	22
R2- North	3500-5500	6.4	666	299 ± 1.5	23 ± 1.4	0.48 ± 0.69	8
R3- Center-North	4100-6900	5.9	1136	514 ± 2.6	156 ± 9.3	0.58 ± 0.83	21
R4- Center-West	4000-5200	0.6	107	12 ± 0.06	15 ± 0.9	0.24 ± 0.29	42

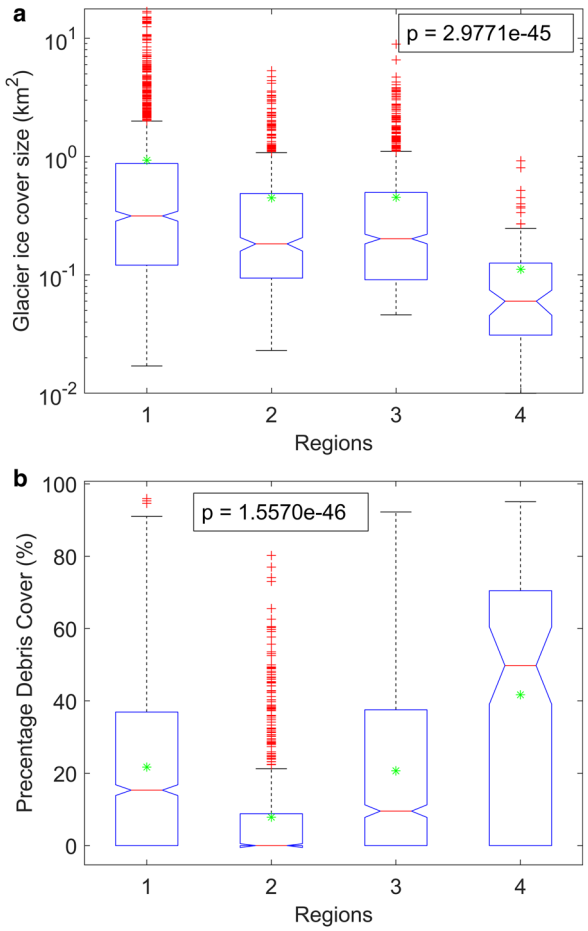

Fig. 4. Box plots of glacier ice cover size a) and percentage debris cover b) at four regions. The upper and lower box margins mark the 75th (Q75) and the 25th (Q25) quartiles respectively, with the mid box line showing the median. The whiskers show the extremes of the data (maximum and minimum) except for situations where outliers are present, defined as either Q75 + 1.5(Q75−Q25) for the maximum and Q25−1.5(Q75−Q25) for the minimum.

debris production are represented more effectively. As with the significant majority of the preceding analyses the principal component that represents glacier length and elevation range is ranked as the first most important in zones 2, 3, 5 and also first but combined with catchment size in zone 6. It is ranked the second most important in zones 1 and 4. The associations with debris cover remain negative. The component representing the glacier width ranked the most important in zone 1 and second in zones 2 and 3, whereas it combined with the variables glacier length and elevation range for other zones and with negative associations.

Components representing catchment size were the fourth most important in zones 2 and 3. In zone 4 the debris influence area in the catchment was ranked as the third most important component. In these three cases there was positive association. In zone 6 and zone 4 (catchment area only) combined with glacier length, width and elevation range and there were negative association signs. These indicate that glaciers with bigger debris influence areas also tend to have higher percentage ice-covered debris while larger catchments do not necessarily have bigger debris influence areas and are more influenced by glacier length, width and elevation range. The principal component that represents variables relating to glacier/catchment slope is ranked third in geological zones 2, 3 and 5 but is not identified for other zones. The positive association with debris cover suggests that glaciers, and their catchments, with steeper slopes tend to have higher percentage ice-covered debris in certain geological zones. The principal component associated with glacier altitude appears only for geological zone 4, and is the most important component and with a negative sign of association.

5. Discussion

5.1 Indices of glacier debris cover

Glaciers in the Himalaya are commonly associated with debris-laden ice avalanches and rockfall onto glacier surfaces from steep surrounding slopes (Shroder and others, 2000; Kaushik and others, 2019). Thus, mapping glacier extent and its change through time needs to take into account debris-covered ice. Paul and others (2015) have reported that errors involved in mapping glaciers can be significant when glaciers are heavily debris-covered and that this is a major challenge for glaciological studies (Shukla and others, 2010; Paul and others, 2015). The complex physical characteristics of debris-covered ice make it difficult to map with optical remote sensing (Holobâcă and others, 2021). Most studies are limited to small geographical regions and where only a small number of glaciers (<5) are analyzed (Robson and others, 2015; Kaushik and others, 2019). Inventories also exist with more specific region-based calibration but these have tended to focus on glaciers >1 km^2 in size (e.g. Scherler and others, 2018; Herreid and Pellicciotti, 2020; Fleischer and others, 2021). In this study, a combination of two thermal indices showed encouraging results for remote sensing of debris-covered ice over a spatially extensive zone. While Lougeay (1974) argued that thicker layers of debris may weaken TIR signals, field data for the Mir Samir Glacier clearly show that signals could be captured under thicker debris cover, even if the maximum depth that can be measured was not established in this study. It emphasizes the value of continued research with thermal infrared data and necessary downscaling methods.

As is standard practice, our NIR and SWIR datasets were corrected for top of the atmosphere effects. However, such correction introduced more noise into the thermal based debris cover index and coarsened the resolution of the outputs (Fig. S5, Supplementary Materials). Thus, we did not correct the thermal band used in (1) for TOA effects. We can justify the lack of correction in three ways. First, we note that converting TIR DNs to TOA is a linear correction process that should not make much difference and which is also undertaken because it is dependent on local meteorological data that are themselves highly uncertain

https://doi.org/10.1017/jog.2023.14 Published online by Cambridge University Press

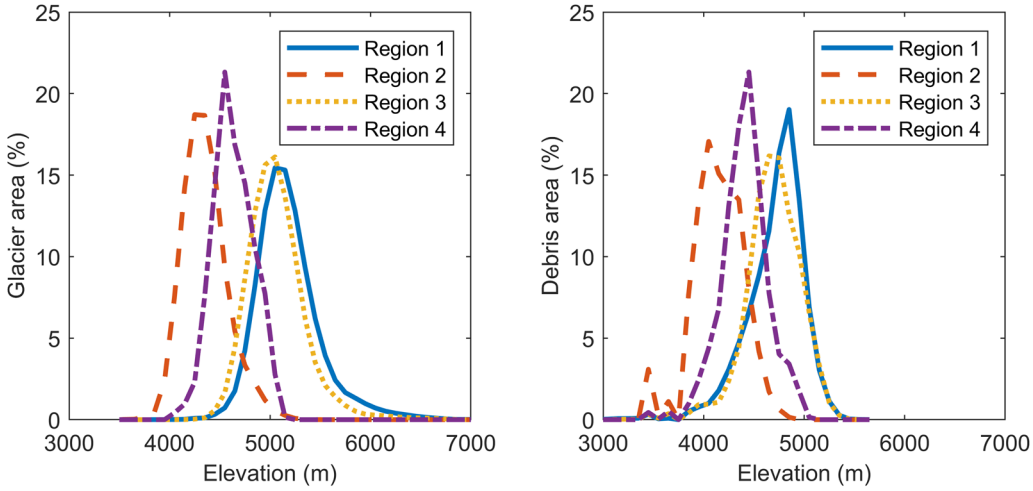

Fig. 5. Hypsometric distribution curve of glaciers (a) and debris cover (b) in percentage grouped in bins of 100 m and by region.

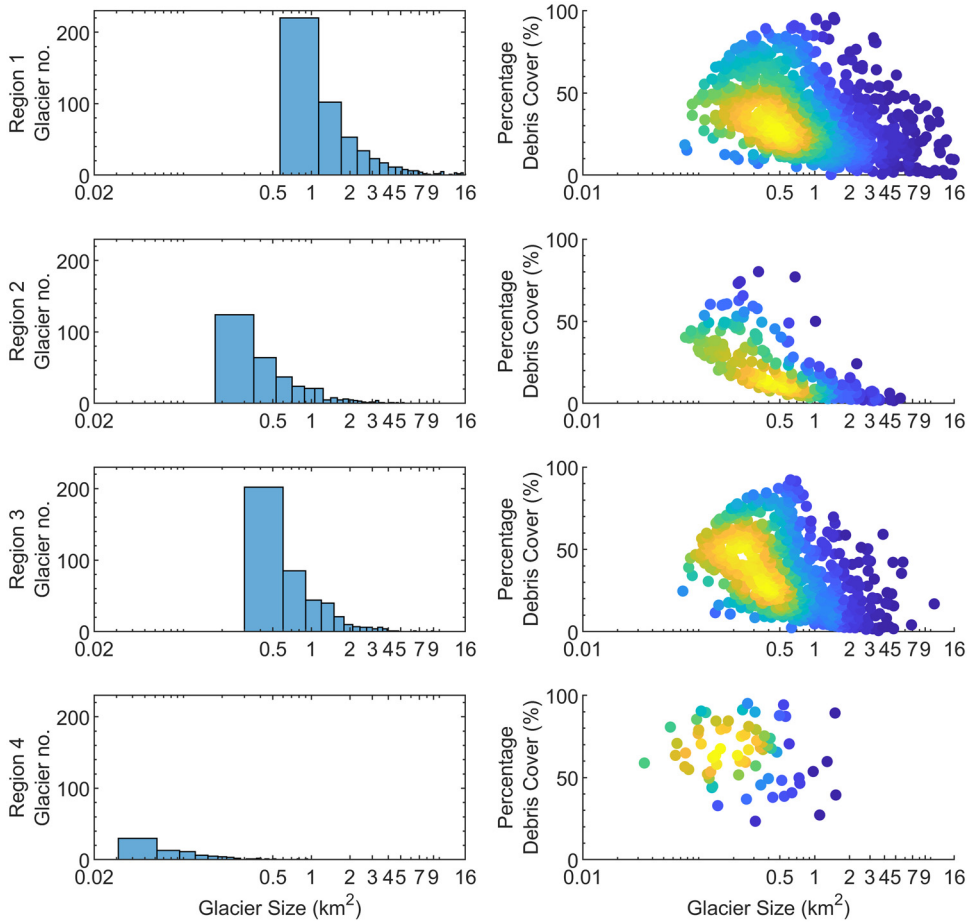

Fig. 6. Description of glacier number by glacier area and plots of percentage debris-covered ice against glacier size for each geographical region show in Figure 1.

especially in remote regions (USGS, 2022). Second, using non atmospheric corrected imagery at high altitudes appears to have minimal influences on mapping (Bishop and others, 2000) and other researchers have obtained better results and transferability using DNs for mapping glaciers (Bhambri and others, 2011; Haireti and others, 2016). Third, we undertook checks by comparing the DN-TOA relationships for different images (Supplementary Material). These showed very little variation in the range of ToA values used for image thresholding, suggesting our index is likely less sensitive to ToA variations and the index thresholds should be transferable. By extending validation to multiple glaciers within Afghanistan and beyond might require ToA correction due to use of images obtained at different times/dates. However, even without ToA correction we did not find a clear pattern of degradation in accuracy statistics (Table 3), and the threshold for identifying debris-covered ice seemed to transfer without further calibration. We nonetheless suggest that this conclusion is checked if this index is applied elsewhere.

Most of the TIR signals suggesting debris-covered ice were associated with igneous rocks (mainly granite and granodiorite)

https://doi.org/10.1017/jog.2023.14 Published online by Cambridge University Press

Table 5. Loadings of each original variables (all dataset) on each principal component with more than 5% contribution to the variance of the original data. Important variables are flagged in bold (correlations >0.7 or <−0.7)

Loadings (all dataset) $R^2 = 43.7\%$	PC1	PC2	PC3	PC4	PC5
Catchment area	**0.760**	0.379	−0.225	0.337	0.252
Catchment mean slope	−0.021	0.063	0.590	−0.351	−0.153
Glacier length	0.454	***0.639***	−0.405	0.235	0.401
Glacier width	0.335	0.367	−0.204	**0.840**	0.028
Debris influence area	**0.975**	0.145	−0.095	0.108	−0.059
Mean altitude	0.029	0.413	0.037	0.034	0.019
Elevation range	0.356	**0.900**	0.005	0.233	−0.061
Glacier slope mean	−0.097	0.158	**0.883**	−0.120	−0.088
Geological hardness grade	−0.045	−0.060	0.207	0.014	0.028
Explained variance (%)	*22.0*	*19.1*	*16.0*	*12.0*	*2.9*
PC added	*/*	*1*	*3*	*2*	*/*
Coefficient		−0.095	0.066	−0.087	
pValue		0.00	0.00	0.00	

Note: Data in bold typeface are identified with correlations >0.7 or <−0.7. (/) indicates variable is not entered into the stepwise regression.

less prone to weathering and leading to coarser and likely drier surface debris. In our case, we identified a second situation where the TIR signal was absent but it was clear that there was debris-covered ice. The second index (2) was crucial for glaciers whose geology was associated with detrital sedimentary rocks, more readily weathered and leading to smaller grain-sizes and a wetter surface. This is an important finding for debris-covered ice mapping from remote sensing, but one that needs further testing.

As with other studies (e.g. Herreid, 2021; Stewart and others, 2021), the real challenge with developing new indices such as ours is obtaining data for calibration and/or validation and calibration suggested that the classification thresholds were important. We found that using a relatively low threshold for the debris cover indices increased the commission error, but using a relatively high threshold increased the omission error (Wang and others, 2020). Therefore, selecting an optimal threshold is still a challenging task. A weakness of this study is having field observations from only one glacier; but the remoteness of glaciers in Afghanistan combined with on-going security problems makes this a challenge. That said, the transferability of the threshold we optimized from field-based calibration to other glaciers (Table 3) is reassuring.

The combination of TIR with panchromatic imagery was central to allowing us to map glaciers much smaller than those typically mapped by others using remote sensing. For instance, Herreid and Pellicciotti (2020) set a minimum glacier size as 1 km^2 and Scherler and others (2018) obtained poorer mapping accuracies for glaciers less than 1 km^2. Figure 6 shows that Afghanistan's glaciers are mainly smaller than 1 km^2. Figure 3 also shows that our indices produce greater extents of debris-covered ice than in published inventories. The presence of crevasses and ponds in these zones confirms that these enlarged zones are indeed ice-cored. The zones tend to be somewhat irregular and also contain holes, commonly where glacier retreat has left exposed bedrock patches, rather than debris-covered ice. This corresponds to the fact that debris-covered ice in High Mountain Asia tends to have a complex morphology and hummocky, rugged topography (Miles and others, 2020).

The identification of more extensive zones of debris-covered ice in our index largely explains why our accuracy statistics are better (Table 3) but these also emphasize a key point. Our goal was to map debris-covered ice, and not simply debris-cover on glaciers. Rapid glacier retreat is likely leading to extensive debris-covered ice that may become progressively disconnected from the glacier. Whether such zones are included as 'glacier' or not is a debatable point. In our case, with a long-term goal of understanding glacier retreat for Afghan water resources, our interest is in debris-covered ice whether or not it remains connected to the glaciers. Thus, we do not argue that our approach is better, rather that it is more appropriate if the scientific goal is mapping debris-covered ice rather than debris cover on glaciers.

5.2 The glacier inventory

We identified 3408 glaciers (⩾0.01 km^2) covering 2,841 ± 51.1 km^2 in area using datasets for 2016. Maharjan and others (2018) identified 3782 glaciers (⩾0.01 km^2) with 2539 km^2 of area for 2015. One year is not enough for these differences to be real and we think that they arise because Maharjan and others (2018) used the normalized difference snow index (NDSI) for glacier mapping and a single slope threshold for mapping debris-covered ice. The larger number of glaciers then relates to the fact that they considered glaciers with size ⩾ 0.01 km^2; and underestimation of glacier area corresponds to the fact that the NDSI could not detect zones of glaciers under shadow as well as ice covered by thicker debris. In addition, the slope threshold of <24°, used by Maharjan and others (2018), may not detect debris cover when the glacier tongue transition to the unglaciated zone is gentle (Paul, 2003; Bolch and Kamp, 2005; Frey and others, 2012).

This study estimated 619 ± 40 km^2 of debris-covered ice for Afghanistan and a total debris cover as a percentage of glacier area of ~ 22%. This is higher than for south-west Asia as a whole (Herreid and Pellicciotti, 2020) but it also masks substantial within-region variation (Table 4) of between 8 and 42% debris cover. It also reflects the fact that we consider debris-covered ice and not just debris-covered glacier.

5.3 Controls on debris cover

Assessment of debris-cover development on Afghan glaciers by principal component analysis showed that considering all glaciers in a single analysis masked sensitivity to certain drivers. Dividing the dataset into two classes based on climate zones and geological zones produced more clear findings. Components that represented variables related to glacier length, width and elevation

Table 6. PCA results based on the complete dataset

Interpretation of the PC	% of original data explained by PC	Loading sign	Sign of association in stepwise regression	Order of addition to stepwise regression (Rank)
PC2. Glacier length and elevation range	19.1%	+	–	1
PC4. Glacier width	12.0%	+	–	2
PC3. Glacier/catchment slope	16.0%	+	+	3
PC1. Catchment size	22.0%	+	/	/
PC5. Glacier altitude			N	

Rows are sorted vertically by importance of contribution to the stepwise regression model. N indicates no PC identified with this interpretation. / indicates not added to the stepwise regression.

https://doi.org/10.1017/jog.2023.14 Published online by Cambridge University Press

Table 7. PCA results based on climatic zone classifications

Interpretation of the PC showing the sign of the loading on each variable	% of original data explained by PC	C Z1 $R^2 = 52\%$		% of original data explained by PC	C Z2 $R^2 = 58\%$		% of original data explained by PC	C Z3 $R^2 = 55\%$		% of original data explained by PC	C Z4 $R^2 = 48\%$		% of original data explained by PC	C Z5 $R^2 = 67\%$	
		Association	Rank		Association	Rank		Association	Rank		Association	Rank		Association	Rank
Glacier length (+)and Elevation range (+)	21	–	1	26	–	1	21	–	1	12	–	2	19	–	1
Catchment size (+)	17	+	5	/			/			/			27	–	4
Glacier width (+)	6	–	2	6	–	2	7	–	3	N			11	–	2
Glacier altitude (+)	10	–	4	/	–	1	/			15	–	1	N		
Glacier/catchment slope (+)	16	+	3	15	+	4	20	+	2	18	+	3	14	+	3

C Z1: Climate zone 1 (Arid, desert, cold).
C Z2: Climate zone 2 (Arid, steppe, cold).
C Z3: Climate zone 3 (Cold, dry summer, hot summer).
C Z4: Climate zone 4 (Cold, dry summer, hot summer, Monsoonal Influence).
C Z5: Climate zone 5 (Temperate, dry summer, hot summer).
N indicates no PC identified with this interpretation. / indicates not added to the stepwise regression.

Table 8. PCA results based on glacier geological zones

Interpretation of the PC	% of original data explained by PC	Geo Z1 $R^2 = 51\%$		% of original data explained by PC	Geo Z2 $R^2 = 54\%$		% of original data explained by PC	Geo Z3 $R^2 = 52\%$		% of original data explained by PC	Geo Z4 $R^2 = 79\%$		% of original data explained by PC	Geo Z5 $R^2 = 54\%$		% of original data explained by PC	Geo Z6 $R^2 = 63\%$	
		Association	Rank		Association	Rank		Association	Rank		Association	Rank		Association	Rank		Association	Rank
Glacier length (+) and Elevation range (+)	18	–	2	23	–	1	20	–	1	43	–	2	26	–	1	45	–	1
Catchment size (+)	24	/		24	+	4	26	+	4				26	/				
Width (+)	22	–	1	11	–	2	10	–	2	N			9	–	2			
Glacier altitude (+)	N			N			N			15	–	1		N			N	
Glacier/catchment slope (+)	20	/		20	+	3	20	+	3	16	/		17	+	3		N	

Geo Z1: Geological zone 1 (Chemical organic).
Geo Z2: Geological zone 2 (Detrital sedimentary).
Geo Z3: Geological zone 3 (Igneous).
Geo Z4: Geological zone 4 (Igneous and detrital sedimentary).
Geo Z5: Geological zone 5 (Metamorphic).
Geo Z6: Geological zone 6 (Metamorphic and igneous).
N indicates no PC identified with this interpretation. / indicates not added to the stepwise regression.

range were uniformly found to be highly important, with bigger glaciers (in terms of length/width) inevitably having a higher range and less debris-covered ice.

Components associated with glacier mean altitude were only found to be important for certain climate zones, notably zones 2 and 5 (Table 7), for geological zone 4 (Table 8). The importance of altitude no doubt reflects the fact that the lower glaciers are more ablation prone and so more prone to accumulating debris, as others observed (e.g. Fleischer and others, 2021). However, the relative lack of importance of altitude-related as compared with size-related components, and the relatively low correlation of altitude with width ($r = 0.281$) and length ($r = 0.233$) emphasizes that altitude is not a primary driver of the extent of debris cover in Afghanistan.

Geology was rarely correlated with significant PCs for the full dataset. However, separating by geological zones resulted in sets of PCs that explained higher proportions of debris cover (Table 8) and clearer and consistent results across zones in terms of the association between components their most correlated variables and debris cover. Few studies have investigated lithological controls on rockfalls and glacier debris cover at regional scales, and data are usually not available for larger areas (Marquinez and others, 2003; Messenzehl and others, 2017; Fleischer and others, 2021). Geological drivers of differences in debris-cover development on glaciers merit further work.

Globally, the relative percentage of debris cover areas systematically decreases from 14% to 0% as glacier size increases although this pattern is not the same for all the regions (Scherler and others, 2018). We found a similar association, albeit with a higher percentage debris cover variation (between 0 and 80%) (Fig. 6). Huang and others (2021) suggested a latitudinal variation with the regional percentage of debris cover a negative exponential function of distance from the equator, implying that warmer climatic zones are more dynamic and conducive to supraglacial debris production. However, orographic factors such as mountain-range, age, relief and lithology may cause regional-scale exceptions to this relation (Herreid and Pellicciotti, 2020).

Chowdhury and others (2021) observed that a relatively gentle slope with lower elevations in ablation areas could be favorable for the abundant accumulation of supraglacial debris. However, for all climate zones and geological zones (Tables 7 and 8) while it is clear that low slopes encourage debris accumulation, our results suggest that steep slopes can also lead to high debris cover likely because of their impacts on sediment production.

6. Conclusion

Using field observations and manual glacier maps, we developed two new indices to map glaciers and debris-covered ice in Afghanistan with promising results. During the mapping process, we were able to distinguish between different debris-covered ice in terms of their geological formations and thermal characteristics. The result of the mapping was a new glacier inventory for Afghanistan. Our analysis, based on 3408 glaciers, showed that Afghan glaciers are highly debris-covered, at 21.7 ± 1.4% of total glacier area, although this varies regionally; regions with smaller glaciers tend to have higher percentage debris cover. The characteristics of glaciers in Afghanistan, and their debris cover, are dependent on climate and geology. Debris cover is predominantly affected by measures of glacier length, width and elevation range; higher values of these measures tend to be associated with glaciers with less debris cover. Catchment size effects are complex and vary by region. The proportion of non glacier area in a catchment appears to an important influence on debris cover development. Drier climates tend to produce higher debris cover as do glaciers in geological zones with more readily-weathered sediment.

Supplementary material. The supplementary material for this article can be found at https://doi.org/10.1017/jog.2023.14.

Acknowledgements. We greatly appreciate and thank Afghanistan government offices that supported this research, special thanks to the Ministry of Energy and Water (MEW) of Afghanistan for facilitating our fieldwork, Ministry of Mines and Petroleum of Afghanistan and Ministry of Agriculture Irrigation and Livestock of Afghanistan for providing us high-resolution spatial datasets. We acknowledge and appreciate Prof. Horst Machguth's contribution for calculating the glacier length for our dataset with his method. This research was supported by Swiss Government Excellence Scholarship Program, we thank them for their continued support. We finally would like to thank three anonymous reviewers and the Scientific Editor Prof. Joseph Shea for having contributed to the improvement of the manuscript.

References

Aiazzi B, Baronti S and Selva M (2007) Improving component substitution pansharpening through multivariate regression of MS + Pan data. *IEEE Transactions on Geoscience and Remote Sensing* **45**(10), 3230–3239. doi: 10.1109/TGRS.2007.901007

ALOS Advanced Land Observing Satellite (2022) Global Digital Surface Model "ALOS World 3D – 30 m (AW3D30)" Available at: https://www.eorc.jaxa.jp/ALOS/en/aw3d30/data/index.htm (Accesses 7 September 2022).

Amani M, Parsian S, MirMazloumi SM and Aieneh O (2016) Two new soil moisture indices based on the NIR-red triangle space of Landsat-8 data. *International Journal of Applied Earth Observation and Geoinformation* **50**, 176–186. doi: 10.1016/j.jag.2016.03.018

Amschwand D and 5 others (2021) Deciphering the evolution of the Bleis Marscha rock glacier (Val d'Err, eastern Switzerland) with cosmogenic nuclide exposure dating, aerial image correlation, and finite element modeling. *The Cryosphere* **15**(4), 2057–2081. doi: 10.5194/tc-15-2057-2021

Bajracharya R and Shrestha R (2011) *The Status of Glaciers in the Hindu Kush-Himalayan Region*. Kathmandu: International Centre for Integrated Mountain Development (ICIMOD).

Benn DI and Owen LA (2002) Himalayan glacial sedimentary environments: a framework for reconstructing and dating the former extent of glaciers in high mountains. *Quaternary International* **97**, 3–25. doi: 10.1016/S1040-6182(02)00048-4

Bhambri R, Bolch T and Chaujar RK (2011) Mapping of debris-covered glaciers in the Garhwal Himalayas using ASTER DEMs and thermal data. *International Journal of Remote Sensing* **32**(23), 8095–8119. doi: 10.1080/01431161.2010.532821

Bhardwaj A, Joshi PK, Singh MK, Sam L and Gupta RD (2014) Mapping debris-covered glaciers and identifying factors affecting the accuracy. *Cold Regions Science and Technology* **106**, 161–174. doi: 10.1016/j.coldregions.2014.07.006

Bishop P and 5 others (2000) Remote-sensing science and technology for studying glacier processes in high Asia. *Annals of Glaciology* **31**, 164–170. doi: 10.3189/172756400781820147

Bishop P, Shroder J and Ward L (1995) SPOT multispectral analysis for producing supraglacial debris-load estimates for Batura glacier, Pakistan. *Geocarto International* **10**(4), 81–90. doi: 10.1080/10106049509354515

Blum WE, Nortcliff S and Schad P (2018) *Essential of Soil Science: Soil Formation, Functions, Use and Classification (World Reference Base, WRB)*. Stuttgart, Germany: Borntraeger Science Publishers. doi: 10.4206/agrosur.2019.v47n1-02

Bodin X, Rojas F and Brenning A (2010) State and recent evolution of the cryosphere in the Andes of Santiago (Chile, 33.5°S). *Geomorphology* **118** (3–4), 453–464. doi: 10.1016/j.geomorph.2010.02.016

Bolch T, Buchroithner MF, Kunert A and Kamp U (2007) Automated delineation of debris-covered glaciers based on ASTER data. *Proceedings of GeoInformation in Europe 27th EARSeL-Symposium*, 4–7 June 2007, Bozen, Italy, M.A. Gomarasca (Ed.), pp. 403–410 (The Netherlands: Millpress). doi: 10.5167/uzh-137197

Bolch T and Kamp U (2005) Glacier mapping in high mountains using DEMs, Landsat and ASTER data. *8th International Symposium on High Mountain Remote Sensing Cartography*, La Paz (Bolivien), 20 March

2005–27 March 2005. Karl-Franzens-Universität Graz, pp. 37–48. doi: 10.5167/uzh-137251

Bolch T and Kamp U (2006) Glacier mapping in high mountains using DEMs, Landsat and ASTER data. *Grazer Schriften der Geographie und Raumforschung* **41**, 37–48.

Choi M (2006) A new intensity-hue-saturation fusion approach to image fusion with a tradeoff parameter. *IEEE Transactions on Geoscience and Remote Sensing* **44**(6), 1672–1682. doi: 10.1109/TGRS.2006.869923

Choi J, Yu K and Kim Y (2010) A new adaptive component-substitution-based satellite image fusion by using partial replacement. *IEEE Transactions on Geoscience and Remote Sensing* **49**(1), 295–309. doi: 10.1109/TGRS.2010.2051674

Chowdhury A, Sharma MC, Kumar S and Debnath M (2021) Glacier changes in the Chhombo Chhu Watershed of the Tista basin between 1975 and 2018, the Sikkim Himalaya, India. *Earth System Science Data* **13**(6), 2923–2944. doi: 10.5194/essd-13-2923-2021

Congalton RG and Green K (2019) *Assessing the Accuracy of Remotely Sensed Data: Principles and Practices*. Florida, FL: CRC Press. doi: 10.1016/j.cageo.2006.05.015.

Ferguson C and Vieli A (2021) Modelling steady states and the transient response of debris-covered glaciers. *The Cryosphere* **15**(7), 3377–3399. doi: 10.5194/tc-15-3377-2021

Fleischer F, Otto JC, Junker RR and Hölbling D (2021) Evolution of debris cover on glaciers of the Eastern Alps, Austria, between 1996 and 2015. *Earth Surface Processes and Landforms* **46**(9), 1673–1691. doi: 10.1002/esp.5065

Foody GM (2002) Status of land cover classification accuracy assessment. *Remote Sensing of Environment* **80**(1), 185–201. doi: 10.1016/S0034-4257(01)00295-4

Frey H, Paul F and Strozzi T (2012) Compilation of a glacier inventory for the western Himalayas from satellite data: methods, challenges, and results. *Remote Sensing of Environment* **124**, 832–843. doi: 10.1016/j.rse.2012.06.020

Ghosh S, Pandey AC and Nathawat MS (2014) Mapping of debris-covered glaciers in parts of the Greater Himalaya Range, Ladakh, western Himalaya, using remote sensing and GIS. *Journal of Applied Remote Sensing* **8**(1), 083579. doi: 10.1117/1.JRS.8.083579

Giese A, Boone A, Wagnon P and Hawley R (2020) Incorporating moisture content in surface energy balance modeling of a debris-covered glacier. *The Cryosphere* **14**(5), 1555–1577. doi: 10.5194/tc-14-1555-2020

Gilbert O, Jamieson D, Lister H and Pendlington A (1969) Regime of an Afghan glacier. *Journal of Glaciology* **8**(52), 51–65. doi: 10.3189/S0022143000020761

Gopalakrishnan R (1982) *The Geography and Politics of Afghanistan*. New Delhi: Concept Publishing Company.

Gupta RP, Tiwari RK, Saini V and Srivastava N (2013) A simplified approach for interpreting principal component images. *Advances in Remote Sensing* **2**(2), 111–119. doi: 10.4236/ars.2013.22015

Haireti A, Tateishi R, Alsaaideh B and Gharechelou S (2016) Multi-criteria technique for mapping of debris-covered and clean-ice glaciers in the Shaksgam valley using Landsat TM and ASTER GDEM. *Journal of Mountain Science* **13**(4), 703–714. doi: 10.1007/s11629-015-3649-9

Herreid S (2021) What can thermal imagery tell us about glacier melt below rock debris? *Frontiers in Earth Science* **9**, 681059. doi: 10.3389/feart.2021.681059

Herreid S and Pellicciotti F (2020) The state of rock debris covering Earth's glaciers. *Nature Geoscience* **13**(9), 621–627. doi: 10.1038/s41561-020-0615-0

Holobâcă IH and 8 others (2021) Multi-sensor remote sensing to map glacier debris cover in the Greater Caucasus, Georgia. *Journal of Glaciology* **67**, 685–696. doi: 10.1017/jog.2021.47

Huang L, Li Z, Zhou JM and Zhang P (2021) An automatic method for clean glacier and nonseasonal snow area change estimation in High Mountain Asia from 1990 to 2018. *Remote Sensing of Environment* **258**, 112376. doi: 10.1016/j.rse.2021.112376

Humlum J, Køie M and Ferdinand K (1959) *La géographie de l'Afghanistan: étude d'un pays aride. etude d'un pays*. Aarhus: Gyldendal.

Jensen JR (1996) *Introductory Digital Image Processing: a Remote Sensing Perspective*. New York, NY: Prentice-Hall Inc.

Jouvet G, Huss M, Funk M and Blatter H (2011) Modelling the retreat of Grosser Aletschgletscher, Switzerland, in a changing climate. *Journal of Glaciology* **57**(206), 1033–1045. doi: 10.3189/002214311798843359

Juen M, Mayer C, Lambrecht A, Wirbel A and Kueppers U (2013) Thermal properties of a supraglacial debris layer with respect to lithology and grain size. *Geografiska Annaler: Series A, Physical Geography* **95**(3), 197–209. doi: 10.1111/geoa.12011

Jung S and Park W (2014) Multi-sensor fusion of Landsat 8 thermal infrared (TIR) and panchromatic (PAN) images. *Sensors* **14**(12), 24425–24440. doi: 10.3390/s141224425

Kääb A and 7 others (2014) Glacier mapping and monitoring using multispectral data. In *Global Land Ice Measurements from Space*. Berlin, Heidelberg: Springer, pp. 75–112. doi: 10.1007/978-3-540-79818-7

Kaushik S, Joshi PK and Singh T (2019) Development of glacier mapping in Indian Himalaya: a review of approaches. *International Journal of Remote Sensing* **40**(17), 6607–6634. doi: 10.1080/01431161.2019.1582114

Lillesand T, Kiefer RW and Chipman J (2015) *Remote Sensing and Image Interpretation*, 7th Edn New York, NY: Wiley.

Lobell DB and Asner GP (2002) Moisture effects on soil reflectance. *Soil Science Society of America Journal* **66**(3), 722–727. doi: 10.2136/sssaj2002.7220

Lougeay R (1974) Detection of buried glacial and ground ice with thermal infrared remote sensing. Advanced Concepts and Techniques in the Study of Snow and Ice Resources. *National Academy of Sciences: Washington, DC, USA*.

Machguth H and Huss M (2014) The length of the world's glaciers–a new approach for the global calculation of center lines. *The Cryosphere* **8**(5), 1741–1755. doi: 10.5194/tc-8-1741-2014

Maharjan SB and 8 others (2018) Status and Decadal Changes of Glaciers in Afghanistan since 1990s. *AGU Fall Meeting Abstracts* 2018, C32A-05.

MAIL (2020) *High Resolution Digital Elevation Model of Afghanistan*. Ministry of Agriculture Irrigation and Livestock of Afghanistan, 1004 – Jamal Mina, Kabul, Afghanistan.

Marquinez J, Duarte RM, Farias P and Sanchez MJ (2003) Predictive GIS-based model of rockfall activity in mountain cliffs. *Natural Hazards* **30**(3), 341–360.

Messenzehl K, Meyer H, Otto JC, Hoffmann T and Dikau R (2017) Regional-scale controls on the spatial activity of rockfalls (Turtmann Valley, Swiss Alps) – A multivariate modeling approach. *Geomorphology* **287**, 29–45. doi: 10.1016/j.geomorph.2016.01.008

Miles E and 5 others (2018) Surface pond energy absorption across four Himalayan glaciers accounts for 1/8 of total catchment ice loss. *Geophysical Research Letters* **45**(19), 10–464. doi: 10.1029/2018GL079678

Miles E and 5 others (2020) Hydrology of debris-covered glaciers in High Mountain Asia. *Earth-Science Reviews* **207**, 103212. doi: 10.1016/j.earscirev.2020.103212

Mölg N, Bolch T, Rastner P, Strozzi T and Paul F (2018) A consistent glacier inventory for Karakoram and Pamir derived from Landsat data: distribution of debris cover and mapping challenges. *Earth System Science Data* **10**(4), 1807–1827. doi: 10.5194/essd-10-1807-2018

MoMP (2020) *Russian geological map of Afghanistan*. Ministry of Mines and Petroleum of Afghanistan, 1004 – Shaheed Abdulhaq Squar, Kabul, Afghanistan.

Nicholson L and Benn DI (2006) Calculating ice melt beneath a debris layer using meteorological data. *Journal of Glaciology* **52**(178), 463–470. doi: 10.3189/172756506781828584

Nicholson LI, McCarthy M, Pritchard HD and Willis I (2018) Supraglacial debris thickness variability: impact on ablation and relation to terrain properties. *The Cryosphere* **12**, 3719–3734. doi: 10.5194/tc-12-3719-2018

Nuimura T and 12 others (2015) The GAMDAM glacier inventory: a quality-controlled inventory of Asian glaciers. *The Cryosphere* **9**(3), 849–864. doi: 10.5194/tc-9-849-2015

Paul F (2003) *The New Swiss Glacier Inventory 2000: Application of Remote Sensing and GIS* (Thesis (Doctoral)). University of Zurich, Zurich, Switzerland. Available at: https://www.zora.uzh.ch/id/eprint/163148/ (Accesses 7 September 2022).

Paul F and 24 others (2015) The glaciers climate change initiative: methods for creating glacier area, elevation change and velocity products. *Remote Sensing of Environment* **162**, 408–426. doi: 10.1016/j.rse.2013.07.043

Paul F, Huggel C and Kääb A (2004) Combining satellite multispectral image data and a digital elevation model for mapping debris-covered glaciers. *Remote Sensing of Environment* **89**(4), 510–518. doi: 10.1016/j.rse.2003.11.007

Paul F, Kääb A, Maisch M, Kellenberger T and Haeberli W (2002) The new remote-sensing-derived Swiss glacier inventory: i. Methods. *Annals of Glaciology* **34**, 355–361. doi: 10.3189/172756402781817941

Peel MC, Finlayson BL and McMahon TA (2007) Updated world map of the Köppen-Geiger climate classification. *Hydrology and Earth System Sciences* **11**(5), 1633–1644. doi: 10.5194/hess-11-1633-2007

https://doi.org/10.1017/jog.2023.14 Published online by Cambridge University Press

Pfeffer T and 19 others (2014) The Randolph Glacier Inventory: a globally complete inventory of glaciers. *Journal of Glaciology* **60**(221), 537–552. doi: 10.3189/2014JoG13J176

Pratap B, Dobhal DP, Mehta M and Bhambri R (2015) Influence of debris cover and altitude on glacier surface melting: a case study on Dokriani Glacier, central Himalaya, India. *Annals of Glaciology* **56**(70), 9–16. doi: 10.3189/2015AoG70A971

Racoviteanu AE, Paul F, Raup B, Khalsa SJS and Armstrong R (2009) Challenges and recommendations in mapping of glacier parameters from space: results of the 2008 Global Land Ice Measurements from Space (GLIMS) workshop, Boulder, Colorado, USA. *Annals of Glaciology* **50** (53), 53–69. doi: 10.3189/172756410790595804

Rai C and Mukherjee R (2021) Spatio-temporal change delineation and forecasting of snow/ice-covered areas of Sikkim Himalaya using multispectral and thermal band combinations of Landsat imagery. *Environmental Challenges* **4**, 100163. doi: 10.1016/j.envc.2021.100163

Raup B and 11 others (2007) Remote sensing and GIS technology in the Global Land Ice Measurements from Space (GLIMS) project. *Computers & Geosciences* **33**(1), 104–125. doi: 10.1016/j.cageo.2006.05.015

Robson BA and 5 others (2015) Automated classification of debris-covered glaciers combining optical, SAR and topographic data in an object-based environment. *Remote Sensing of Environment* **170**, 372–387. doi: 10.1016/j.rse.2015.10.001

Rowan V, Egholm L, Quincey J and Glasser F (2015) Modelling the feedbacks between mass balance, ice flow and debris transport to predict the response to climate change of debris-covered glaciers in the Himalaya. *Earth and Planetary Science Letters* **430**, 427–438. doi: 10.1016/j.epsl.2015.09.004

Scherler D, Bookhagen B and Strecker MR (2011) Spatially variable response of Himalayan glaciers to climate change affected by debris cover. *Nature Geoscience* **4**(3), 156–159. doi: 10.1038/ngeo1068

Scherler D, Wulf H and Gorelick N (2018) Global assessment of supraglacial debris-cover extents. *Geophysical Research Letters* **45**(21), 11–798. doi: 10.1029/2018GL080158

Shokory JS, Schaefli B and Lane SN (2023) Water resources and related hazards under rapid climate warming: a review of Afghanistan. Forthcoming in *Hydrological Sciences Journal* **68**, 507–525.

Shroder JF (1978) Remote sensing of Afghanistan. *Afghanistan Journal* **5**(4), 123–128.

Shroder JF (1980) Special problems of glacier inventory in Afghanistan. *International Association of Hydrological Sciences Publication* **126**, 149–154.

Shroder JF (2014) *Natural Resources in Afghanistan: Geographic and Geologic Perspectives on Centuries of Conflict*. California, CA: Elsevier.

Shroder JF and Ahmadzai SJ (2016) *Transboundary Water Resources in Afghanistan: Climate Change and Land-use Implications*. Amsterdam: Elsevier.

Shroder JF and Bishop MP (2010) *Glacier of Asia-Glaciers of Afghanistan*. U.S. In: Williams RS Jr. and Ferrigno JG (Eds), Satellite image atlas of glaciers of the world – Asia: U.S. Geological Survey Professional Paper 1386-F-3. Available at: https://pubs.usgs.gov/pp/p1386f/pdf/F3_Afghanistan.pdf (Accessed 7 September 2022).

Shroder JF, Bishop MP, Copland L and Sloan VF (2000) Debris-covered glaciers and rock glaciers in the Nanga Parbat Himalaya, Pakistan. *Geografiska Annaler: Series A, Physical Geography* **82**(1), 17–31. doi: 10.1111/j.0435-3676.2000.00108.x

Shukla A, Arora MK and Gupta RP (2010) Synergistic approach for mapping debris-covered glaciers using optical–thermal remote sensing data with inputs from geomorphometric parameters. *Remote Sensing of Environment* **114**(7), 1378–1387. doi: 10.1016/j.rse.2010.01.015

Stewart L and 6 others (2021) Using climate reanalysis data in conjunction with multi-temporal satellite thermal imagery to derive supraglacial debris thickness changes from energy-balance modelling. *Journal of Glaciology* **67** (262), 366–384. doi: 10.1017/jog.2020.111

Story M and Congalton R (1986) Accuracy assessment: a user's perspective. *Photogrammetric Engineering and Remote Sensing* **52**, 397–399.

Taschner S and Ranzi R (2002) Comparing the opportunities of Landsat-TM and Aster data for monitoring a debris-covered glacier in the Italian Alps within the GLIMS project. *IEEE International Geoscience and Remote Sensing Symposium* **2**, 1044–1046. doi: 10.1109/IGARSS.2002.1025770

Tielidze LG and 5 others (2020) Supra-glacial debris cover changes in the Greater Caucasus from 1986 to 2014. *The Cryosphere* **14**, 585–598. doi: 10.5194/tc-14-585-2020

USGS (2022) Using the USGS Landsat Level-1 Data Product. United States Geological Survey. Available at: https://www.usgs.gov/landsat-missions/using-usgs-landsat-level-1-data-product (Accessed 7 September 2022).

Veettil BK, Bremer UF, Grondona AEB and De Souza SF (2014) Recent changes occurred in the terminus of the debris-covered Bilafond glacier in the Karakoram Himalayas using remotely sensed images and digital elevation models (1978–2011). *Journal of Mountain Science* **11**(2), 398–406. doi: 10.1007/s11629-013-2677-6

Vincent C and 10 others (2016) Reduced melt on debris-covered glaciers: investigations from Changri Nup Glacier, Nepal. *The Cryosphere* **10**(4), 1845–1858. doi: 10.5194/tc-10-1845-2016

Wang X, Gao X, Zhang X, Wang W and Yang F (2020) An automated method for surface ice/snow mapping based on objects and pixels from Landsat imagery in a mountainous region. *Remote Sensing* **12**(3), 485. doi: 10.3390/rs12030485

Zhang Y, Fujita K, Liu S, Liu Q and Nuimura T (2011) Distribution of debris thickness and its effect on ice melt at Hailuogou glacier, southeastern Tibetan Plateau, using in situ surveys and ASTER imagery. *Journal of Glaciology* **57**(206), 1147–1157. doi: 10.3189/002214311798843331

Zollinger S (2003) Ableitung von Parametern für die Identifikation und Beobachtung gefährlicher Gletscherseen in Nepal aus ASTER Satellitendaten (Doctoral dissertation, Verlag nicht ermittelbar).

https://doi.org/10.1017/jog.2023.14 Published online by Cambridge University Press